Title: Advanced MRI to Differentiate Schwannomas and Metastases in the Cerebellopontine Angle/Internal Auditory Canal

Running title: Schwannoma vs metastasis: Utility of DWI and DCE-MRI

Authors:

Yoshiaki Ota, MD[1], Eric Liao, MD[1], Raymond Zhao[1], Remy Lobo, MD[1], Aristides A Capizzano, MD[1], Jayapalli Rajiv Bapuraj, MD[1], Gaurang Shah, MD[1], Akira Baba, MD, PhD[1], and Ashok Srinivasan, MD[1]

[1]Division of Neuroradiology, Department of Radiology, University of Michigan, 1500 E Medical Center Dr, UH B2, Ann Arbor, MI 48109, USA

Keywords: DWI; DCE-MRI; schwannoma; metastasis, CPA

Corresponding author: Yoshiaki Ota

1500 E Medical Center Dr, UH B2, Ann Arbor, MI 48109, USA

Phone: 7348825904 FAX number: 7346159800

Email address: yoshiako@med.umich.edu

Funding: There was no funding or grant support for this study.

Abstract

Background and Purpose: Differentiating schwannomas and metastases in the cerebellopontine angles (CPA)/internal auditory canals (IAC) can be challenging. This study aimed to assess the role of diffusion weighted imaging (DWI) and dynamic contrast-enhanced MRI (DCE-MRI) to differentiate schwannomas and metastases in the CPA/IAC.

Methods: We retrospectively reviewed 368 patients who were diagnosed with schwannomas or metastases in the CPA/IAC between April 2017 and February 2022 in a single academic center. Forty-three patients had pretreatment DWI and DCE-MRI along with conventional MRI. Normalized mean apparent diffusion coefficient ratio (nADCmean) and DCE-MRI parameters of fractional plasma volume (Vp), flux rate constant (Kep), and forward volume transfer constant were compared along with patients' demographics and conventional imaging features between schwannomas and metastases as appropriate. The diagnostic performances and multivariate logistic regression analysis were performed using the significantly different values.

Results: Between 23 schwannomas (15 males; median 48 years) and 20 metastases (9 males; median 61 years), nADCmean (median 1.69 vs 1.43; P= .002), Vp (median 0.05 vs 0.20; P< .001), and Kep (median 0.41 vs 0.81 minute^{-1}; P< .001) were significantly different. The diagnostic performances of nADCmean, Vp, and Kep were 0.77, 0.90, and 0.83 area under the curves, with cut-off values of 1.68, 0.12, and 0.53, respectively. Vp was identified as the most significant parameter for the tumor differentiation in the multivariate logistic regression analysis (P< .001).

Conclusions: DWI and DCE-MRI can help to differentiate CPA/IAC schwannomas and metastases, and Vp is the most significant parameter.

Introduction

Cerebellopontine angle (CPA) and internal auditory canal (IAC) tumors are the most common neoplasms in the posterior fossa and comprise 6-10% of intracranial tumors.[1,2] The most common tumors in the CPA/IAC are vestibular schwannomas with approximately 80% of incidence,[1,3] followed by meningiomas with 10-15% incidence.[2] Schwannomas are benign nerve sheath tumors, and conventional MRI and CT typically show a homogeneously enhancing mass with cystic changes and sometimes dumbbell-shaped appearance, depending on location.[3,4] These imaging findings are not specific and can be mimicked by brain metastases.[5,6] Isolated or leptomeningeal metastases in the CPA/IAC have been reported, and common primary cancers include melanomas, lung cancers, and breast cancers.[5,6] Although the incidence of metastases is approximately 2%, which is relatively low when compared to benign tumors in the CPA/IAC such as schwannomas and meningiomas, discrimination between CPA/IAC benign tumors and metastases is highly important in terms of patients' care because the treatment strategies are so vastly different.[6,7] Clinically, CPA/IAC metastases often demonstrate acute onset with rapid symptomatic progression, compared to other benign tumors.[5,6] However, aggressive features are not always obvious initially, and the clinical course of schwannomas can be progressive as well, particularly when they are associated with underlying NF2 gene mutation.[8-10] Therefore, clinical differentiation of these two entities can be difficult. In addition, imaging findings can overlap between CPA/IAC benign tumors and metastases, and differentiation on the basis of conventional imaging only can be challenging, especially in the setting of an aggressive CPA/IAC mass without known primary cancer. Multiple intracranial lesions can suggest metastases, but even in this setting, there is a possibility that the CPA lesion represents a superimposed schwannoma or other incidental benign lesion. Therefore, a more precise diagnostic

tool is needed.

Diffusion weighted imaging (DWI) and dynamic contrast-enhanced MRI (DCE-MRI) have been used for characterization of tumor cellularity and unique microstructure, and tumor microvascularity and permeability, respectively,[11-17] and increasingly applied for tumor differentiation and evaluation of treatment effects.[13,18-20] The utility of DCE-MRI for differentiation of schwannomas and meningiomas in the CPA and jugular foramen has previously been shown to be effective with promising diagnostic performances.[13] Based on the fact that different tumors possess distinct internal histoarchitecture, microvascularity, and permeability, we hypothesized that DWI and DCE-MRI can help to differentiate CPA schwannomas and metastases.

In this study, we investigated the role of DWI and DCE-MRI to differentiate CPA schwannomas and metastases in combination with conventional MRI imaging features.

Methods

Study population

Our institutional review board approved this retrospective single-center research study and waived the requirement for informed consent. Data were acquired in compliance with all applicable Health Insurance Portability and Accountability Act regulations. We retrospectively reviewed clinical records and imaging from 368 patients with pathologically confirmed schwannomas and metastases in the CPA/IAC at our institution between April 2017 and February 2022. We excluded patients who did not have pre-treatment MRI including DWI and DCE-MRI (n= 315), whose pre-treatment MRI imaging quality was too poor to evaluate (n = 6) or whose maximal diameters of CPA/IAC lesions were too small (less than 10 mm) to encompass a region of interest (ROI) (n=4). Regarding patients with metastases, there were 2 patients who had bilateral CPA lesions, and the only lesion which was biopsied was included in this study.

In total, 43 patients (24 males, 19 females; age 18-80 years) including 23 patients with schwannomas and 20 patients with metastases were included in this study.

MRI scanning protocol

All MRI examinations were performed using 1.5T or 3T (Ingenia; Philips, Eindhoven) using a 16-channel neurovascular coil. Acquired sequences included axial T2 weight image (WI), axial T1WI, axial fluid-attenuated inversion recovery (FLAIR), and axial pre- and postcontrast 3D-T1WI.

DWI acquisition

DWI was obtained utilizing echo-planar imaging with the following DWI parameters: echo time range: 58–106 ms; repetitive time range: 5000–8500 ms; number of excitations: 1; slice thickness and gap: 3.5–4 and 0–1 mm; field of view: 220–240 mm; matrix size 128 × 128 – 200 × 200, and 3 diffusion directions. Sensitizing diffusion gradients were sequentially applied. B values were 0 and 1000 s/mm^2.

DCE-MRI acquisition

A DCE-MRI sequence was performed using a 3-dimensional T1-weighted fast field echo technique using a 16-channel NeuroVascular coil. 20 ml of gadobenate dimeglumine (Multihance, Bracco diagnostics, Singen, Germany) was administered through a peripheral arm vein. A power injector was used at a flow rate of 5.0 mL/s, followed by a 20 mL saline flush. Sequentially, a DCE-MRI was acquired with the following parameters of 3D-T1 FEE: echo time, 1.86 ms; repetitive time, 4.6 ms; flip angle, 30°; slice thickness, 5.0 mm; field of view, 240×240 mm^2; voxel size, 1.0×1.0×5.0 mm^3; number of excitations, 1; number of slices per dynamic scan, 48 slices; temporal resolution; 8.4 seconds; dynamic phase, 30 dynamics; total acquisition time, 4 mins and 24 seconds.

Patient demographics

Patient demographics included age at diagnosis, sex, main location of the lesion (CPA or IAC), and histological diagnosis from the medical record. In addition, primary cancer and presence of other brain metastatic lesions were recorded in cases of metastases from the medical records.

Imaging processing and analysis

Two board-certified radiologists with 7 (Y.O.) and 10 (E.L.) years of experience reviewed and evaluated conventional imaging findings with consensus, and performed DWI and DCE-MRI analyses independently. The clinical information, histopathological results, and imaging results were blinded to the two readers.

Conventional imaging analysis

Maximal diameter of the tumors was assessed on post-contrast axial 3D-T1WI. As binary variables, cystic or necrotic changes (yes or no) were recorded, using a combination of axial T1WI, T2WI, FLAIR, and pre- and post-contrast T1WI. As well, the enhancement pattern (homogenous versus heterogenous) was evaluated on pre- and postcontrast 3D-T1WI. Adjacent parenchymal edematous change in the brainstem or cerebellum (yes or no) was evaluated on T2WI and FLAIR when lesions were location in the CPA.

DWI analysis

A single freehand region of interest (ROI) was manually drawn on the axial postcontrast 3D-T1WI at the slice of greatest axial diameter, encompassing areas of solid enhancement and taking care to avoid cystic or necrotic areas as well as adjacent vasculature. To avoid volume averaging artifact, the peripheral 2 mm of the lesions was excluded. ADC maps were constructed using commercially available software (Olea Sphere, Version 3.0; Olea Medical). The corresponding ROIs were again contoured on the ADC map with reference to axial postcontrast 3D-T1WI, and adjusted to exclude geometric artifact as needed. As an internal control, a ROI was placed within the medulla oblongata. A normalized mean Apparent Diffusion Coefficient ratio (nADCmean) was calculated by dividing each lesion's ADC value by the ADC value of the medulla oblongata to adjust for the variation of parameters and magnetic field strengths.

DCE-MRI analysis

DCE-MRI analysis also was performed using the Olea Sphere 3.0 software. An arterial input function (AIF) was automatically computed. The permeability module was based on the extended Tofts model, and pixel-based parameter maps were calculated from time intensity curves (TICs). ROIs were placed using the same method used for the DWI analysis. Quantitative parameters fractional plasma volume (Vp), flux rate constant (Kep), and forward volume transfer constant (Ktrans) were calculated. While this process was automated, the corresponding attenuation time curves that demonstrated a rapid increase in attenuation with sharp peaks were deemed appropriate and accurate for analysis. A representative case of DWI and DCE-MRI analysis was shown in Fig. 1.

Statistical analysis

nADCmean, and Vp, Kep, and Ktrans were compared between schwannomas and metastases in the CPA by Mann-Whitney U test and described as medians (interquartile range [IQR]). Regarding the patients' demographics, sex and main location (CPA or IAC) was compared by the Fisher exact test, and age was compared by the Mann-Whitney U test. Conventional imaging features such as cystic/necrotic changes, enhancement patterns, and adjacent edematous changes, were described as the binary variables and compared by the Fisher exact test. For statistically significant values between CPA schwannomas and metastases, receiver operating characteristics (ROC) analysis was performed with the optimal cutoff values, which were determined to maximize the Youden index (sensitivity + specificity - 1). Multivariate logistic regression analysis was performed to identify the most significant parameter to distinguish CPA schwannomas and metastases, with the forward stepwise selection method, where the statistically significant values with a P value of < 0.05 were applied. The intraclass correlation coefficient was used to assess the interobserver agreement for DWI and DCE-MRI parameters. All statistical calculations were conducted using R software (version 4.1.1; R Core Team, Vienna, Austria). Variables with P-values of < 0.05 were considered statistically significant.

Results

Patient demographics and conventional imaging features

Patient demographics and conventional imaging features were summarized in Table 1. There were 23 CPA/IAC schwannomas (sex, 15 males, 8 females; age, median 48 years [39–60]) and 20 metastases (sex, 9 males, 11 females; age, median 61 years [46–66]). There were no significant differences in age, sex, maximal diameter of the tumor, or main location (CPA or IAC) between schwannomas and metastases (P= .12, .23, .30 and .50, respectively). In metastases, 8 breast cancers, 6 lung cancers, 4 melanomas, 2 squamous cell carcinomas of tongue were identified as the primary cancers. Additional intracranial metastatic lesions were identified in 7 out of 20 cases.

Regarding conventional imaging features, there was no significant difference in the presence of cystic/necrotic changes, enhancement pattern (homogeneous versus heterogeneous), or adjacent parenchymal edematous change between schwannomas and metastases (cystic/necrotic changes, 9/23 vs 10/20; P= .55, homogenous versus heterogeneous enhancement, 12/23 vs 4/20; P= .056, adjacent edematous change, 5/16 vs 8/16; P= .47, respectively).

DWI and DCE-MRI analysis

Table 2 represents the comparisons of DWI and DCE-MRI quantitative parameters between CPA/IAC schwannomas and metastases. nADCmean was significantly different between schwannomas and metastases (median 1.69 [1.55-2.0] vs 1.43 [1.12-1.61]; P= .003). Vp and Kep were significantly different between schwannomas and metastases (Vp, median 0.05 [0.03-0.09] vs 0.20 [0.13-0.23]; P< .001, Kep, median 0.41 [0.36-0.48] vs 0.81 [0.62-1.24] $minute^{-1}$; P< .001, respectively). There was no significant difference in Ktrans between CPA/IAC schwannomas and metastases (median 0.18 [0.12-0.23] vs 0.22 [0.15-0.41] $minute^{-1}$; P= 0.52). Representative cases of CPA/IAC schwannomas and metastases are demonstrated in Fig. 2 and Fig 3.

Diagnostic performance based on ROC analysis are summarized in Table 3 and Fig. 4. nADCmean showed 0.77 area under the curve (AUC), 0.57 sensitivity, and 0.90 specificity with a cut-off value of 1.68, while Vp and Kep showed 0.90 and 0.83 AUCs, 1.0 and 0.83 sensitivity, and 0.75 and 0.80 specificity, with cut-off values of 0.12 and 0.53. In multivariate logistic regression analysis, Vp was identified as the most significant parameter between CPA/IAC schwannomas and metastases (P< .001).

Inter-reader agreement

The intraclass correlation coefficient for nADCmean, Vp, Kep, and Ktrans was almost perfect (nADCmean= 0.96, Vp= 0.97, Kep= 0.95, Ktrans= 0.94, respectively).

Discussion

In this retrospective study, we explored the role of DWI and DCE-MRI for the differentiation of CPA/IAC schwannomas and metastases. Patient demographics and conventional imaging did not show any significant differences between schwannomas and metastases, while DWI and DCE-MRI analysis both revealed significant differences between them. nADCmean showed 0.77 AUC, and Kep and Vp provided 0.83 and 0.90 AUCs. Among the significant DWI and DCE-MRI parameters, Vp was shown to be the most promising parameter to differentiate the two tumor types in multivariable logistic regression analysis.

Regarding the patients' demographics, there was no significant difference in age, sex, size of the tumors, and main locations of the lesions. In both groups, the lesions were more commonly found in the CPA than in the ICA (schwannomas 16/23 and metastases 16/20, respectively). Presenting symptoms of CPA/IAC masses are dependent on the size and location.[21] These may present with unilateral sensorineural hearing loss, tinnitus, or vertigo when the lesions are located in IAC.[9,21] However, when the tumor involves the CPA, clinical manifestations of brainstem or cerebellar

compression, as well as obstructive hydrocephalus due to effacement of the fourth ventricle can be seen,[21] which could make the CPA lesions more likely investigated by imaging than the IAC lesions. In the group of metastases, lung cancers, breast cancer, and melanoma were identified as primary cancers in this study. Included primary cancers are consistent with previous studies where these tumors were also considered as common CPA metastases.[7,9] In this study, 35% (7/20) of CPA/IAC metastases were accompanied by other metastatic lesions in the brain. Multiplicity of lesions can favor a diagnosis of metastases.[3,6] However, more than a half of metastases showed only a solitary CPA mass in our study. Therefore, the presence of additional intracranial metastatic lesions was not considered to be a reliable differentiating factor.

Regarding MRI imaging features, cystic/necrotic changes and enhancement pattern showed no significant differences between CPA/IAC schwannomas and metastases, indicating that they are not reliable for differentiation of CPA/IAC schwannomas and metastases, as has been previously suggested.[6] As well, subjacent parenchymal edematous changes involving the underlying brainstem or cerebellum were without significant differences between CPA schwannomas and metastases, suggesting that conventional MRI imaging features are not reliable when differentiating CPA schwannomas form CPA metastases.

Regarding DWI analysis, nADCmean was lower in metastases than in schwannomas with 0.77 AUC with cutoff of 1.68. Historically, schwannomas show high cellular Antoni A and less cellular Antoni B component,[22] and larger schwannomas are likely to undergo cystic changes,[23] which might contribute to higher ADC value than metastases. On the other hand, malignant tumors generally show high cellularity, which is assumed to be a factor contributing to lower ADC values,[12] although this can depend on the type of the primary cancer.[24,25] The primary cancers in our study included breast cancer, lung cancer, melanoma, and squamous cell carcinoma, all of which showed lower ADC values in a previous study,[26] and are commonly encountered metastases in the CPA/IAC region.[6,7,9] Although the result of DWI analysis would require further validation by larger studies which

incorporate more patients, the result of lower ADC values in metastases than in schwannomas could potentially be generalized and used for differentiation of schwannomas and the most frequently encountered metastases in the CPA/IAC. Our study applied the mean ADC value for DWI analysis. The mean ADC value has been the most used parameter for tumor differentiation and assessment/prediction of treatment response.[27] In addition, given that we normalized the mean ADC value to control for variation between different magnetic field strengths and parameters, and the intraclass correlation coefficient of nADCmean was 0.96, the result of nADCmean is believed to make the results of DWI analysis applicable and robust.

Regarding DCE-MRI analysis, Vp and Kep showed significantly higher values in metastases than in schwannomas with 0.90 and 0.83 AUCs with cutoffs of 0.12 and 0.53. Vp and Kep can represent markers of microvascularity and permeability respectively, suggesting that CPA/IPA metastases can show higher microvascularity and permeability than CPA/IAC schwannomas based on our study. DCE-MRI has been recently utilized for head and neck regions including infratentorial extra-axial tumors.[10,13,14,20] One study showed that schwannomas can be differentiated from meningiomas by Vp and Ktrans.[13] However, infratentorial extra-axial malignant tumors have not been adequately investigated. Metastases are most common malignant tumors in the CPA/ICA,[28] so differentiating metastases from schwannomas, which is most common CPA/IAC tumor, is clinically important as the management and treatment strategy of metastases is quite different from that of schwannomas.[7] Different primary malignancies can show distinct DCE-MRI parameters based on their own microvascularity and permeability,[29] but our cohort included common primary cancers of lung cancers, breast cancers, and melanoma,[6,7,9] suggesting that this result could be applicable to the most commonly encountered metastases. In addition, Vp, which represents microvascularity, was the most promising differentiator between the two tumors, suggesting that microvascularity could be a more reliable tumor characteristic for the differentiation of schwannomas and metastases than permeability or internal microstructure.

Clinically, metastasis involvement at the CPA/IAC is suspected based on rapidly progressive cranial nerve deficits, bilateral disease, and history of primary cancer.[7] When metastases are clinically suspected in the abovementioned clinical settings, adding DWI and DCE-MRI sequences to the protocol can be beneficial in differentiation and thus aid in determining appropriate clinical workup and treatment.

There were several limitations in this study. First, this retrospective study was conducted at a single institution with a relatively small cohort. In addition, there are only 20 cases of metastases with 4 different primary cancer, and each metastatic type comparison were not able to be performed. Second, we included heterogeneous primary cancer diseases in metastases, although this heterogeneous group comprised the most commonly encountered metastases. Third, 1.5 T and 3 T scanners were used for this study which might add heterogeneity to the calculated quantitative DCE-MRI parameters. Forth, volume of interest (VOI) analysis was not applied in our study. VOI analysis might reduce the possibility of sampling error, but it is time-intensive and cannot avoid inclusion of necrotic or cystic areas when encompassing the regions of interest. In addition, ROI-based analysis is widely used and easily applied in clinical settings compared to VOI-analysis.

In conclusion, DWI and DCE-MRI sequences can help to differentiate CPA/IAC schwannomas and metastases. When metastases are clinically suspected, including DWI and DCE-MRI sequences to the protocol may be warranted.

Acknowledgements and Disclosure: The authors declare no conflicts of interest.

Reference

1. Bonneville F, Savatovsky J, Chiras J. Imaging of cerebellopontine angle lesions: an update. Part 1: enhancing extra-axial lesions. Eur Radiol 2007;17:2472-82

2. Lin EP, Crane BT. The management and imaging of vestibular schwannomas. AJNR Am J Neuroradiol 2017;38:2034-43

3. Bonneville F, Sarrazin JL, Marsot-Dupuch K, et al. Unusual lesions of the cerebellopontine angle: a segmental approach. Radiographics 2001;21:419-38

4. Skolnik AD, Loevner LA, Sampathu DM, et al. Cranial nerve schwannomas: diagnostic imaging approach. Radiographics 2016;36:1463-77

5. Chiong Y, Mulroy L, Fleetwood IG, et al. Isolated metastasis to the cerebellopontine angle secondary to breast cancer. Can J Surg 2009;52:E213-4

6. Yuh WT, Mayr-Yuh NA, Koci TM, et al. Metastatic lesions involving the cerebellopontine angle. AJNR Am J Neuroradiol 1993;14:99-106

7. Warren FM, Shelton C, Wiggins RH 3rd, et al. Imaging characteristics of metastatic lesions to the cerebellopontine angle. Otol Neurotol 2008;29:835-8

8. Coy S, Rashid R, Stemmer-Rachamimov A, et al. An update on the CNS manifestations of neurofibromatosis type 2. Acta Neuropathol 2020;139:643-65

9. Lakshmi M, Glastonbury CM. Imaging of the cerebellopontine angle. Neuroimaging Clin N Am 2009;19:393-406

10. Ota Y, Liao E, Capizzano AA, et al. Neurofibromatosis type 2 versus sporadic vestibular schwannoma: The utility of MR diffusion and dynamic contrast-enhanced imaging. J Neuroimaging 2022;32:554-60.

11. Gaddikeri S, Gaddikeri RS, Tailor T, et al. Dynamic contrast-enhanced MR imaging in head and neck cancer: techniques and clinical applications. AJNR Am J Neuroradiol 2016;37:588-595

12. Surov A, Meyer HJ, Wienke A. Apparent Diffusion coefficient for distinguishing between malignant and benign lesions in the head and neck region: a systematic review and meta-analysis. Front Oncol 2019;9:1362

13. Ota Y, Liao E, Capizzano AA, et al. MR diffusion and dynamic-contrast enhanced imaging to distinguish meningioma, paraganglioma, and schwannoma in the cerebellopontine angle and jugular foramen. J Neuroimaging 2022;32:502-10.

14. Ota Y, Liao E, Capizzano AA, et al. Diagnostic role of diffusion-weighted and dynamic contrast-enhanced perfusion MR imaging in paragangliomas and schwannomas in the head and neck. AJNR Am J Neuroradiol 2021;42:1839-46

15. Ota Y, Naganawa S, Kurokawa R, et al. Assessment of MR imaging and CT in differentiating hereditary and nonhereditary paragangliomas. AJNR Am J Neuroradiol 2021;42:1320-6

16. Ota Y, Moore AG, Spector ME, et al. Prediction of wound failure in patients with head and neck cancer treated with free flap reconstruction: utility of CT perfusion and MR perfusion in the early postoperative period. AJNR Am J Neuroradiol 2022;43:585-91

17. Tamilchelvan P, Boruah DK, Gogoi BB, et al. Role of MRI in differentiating various posterior cranial fossa space-occupying lesions using sensitivity and specificity: a prospective study. Cureus 2021;13:e16336

18. Ota Y, Liao E, Kurokawa R, et al. Diffusion-weighted and dynamic contrast-enhanced MRI to assess radiation therapy response for head and neck paragangliomas. J Neuroimaging 2021;31:1035-43

19. Chawla S, Kim S, Dougherty L, et al. Pretreatment diffusion-weighted and dynamic contrast-enhanced MRI for prediction of local treatment response in squamous cell carcinomas of the head and neck. AJR Am J Roentgenol 2013;200:35-43

20. Chawla S, Loevner LA, Kim SG, et al. Dynamic contrast-enhanced MRI-derived intracellular water lifetime (tau i): a prognostic marker for patients with head and neck squamous cell carcinomas. AJNR Am J Neuroradiol 2018;39:138-44

21. Yadav P, Jantre M, Thakkar D. Magnetic resonance imaging of cerebellopontine angle lesions. Med J DY Patil Univ 2015;8:751-9

22. Behuria S, Rout TK, Pattanayak S. Diagnosis and management of schwannomas originating from the cervical vagus nerve. Ann R Coll Surg Engl 2015;97:92-7

23. Mehrotra N, Behari S, Pal L, et al. Giant vestibular schwannomas: focusing on the differences between the solid and the cystic variants. Br J Neurosurg 2008;22:550-6

24. Jung WS, Park CH, Hong CK, et al. Diffusion-weighted imaging of brain metastasis from lung cancer: correlation of MRI parameters with the histologic type and gene mutation status. AJNR Am J Neuroradiol 2018;39:273-9

25. Hayashida Y, Hirai T, Morishita S, et al. Diffusion-weighted imaging of metastatic brain tumors: comparison with histologic type and tumor cellularity. AJNR Am J Neuroradiol 2006;27:1419-25

26. Zakaria R, Das K, Radon M, et al. Diffusion-weighted MRI characteristics of the cerebral metastasis to brain boundary predicts patient outcomes. BMC Med Imaging 2014;14:26

27. Chawla S, Kim S, Wang S, Poptani H. Diffusion-weighted imaging in head and neck cancers. Future Oncol 2009;5:959-75.

28. Moffat DA, Ballagh RH. Rare tumours of the cerebellopontine angle. Clin Oncol (R Coll Radiol) 1995;7:28-41

29. Hatzoglou V, Tisnado J, Mehta A, et al. Dynamic contrast-enhanced MRI perfusion for differentiating between melanoma and lung cancer brain metastases. Cancer Med 2017;6:761-7

Tables

Table 1: Patient demographics and conventional imaging features between schwannomas and metastases in the CPA/IAC

	Schwannomas	Metastases	p-value
Numbers of lesions	23	20	NA
Sex (male : female)	15 : 8	9 : 11	.23
Age (year)	48 (39–60)	61 (46–66)	.12
Maximum diameter (mm)	18 (14–31)	17 (11 – 22)	.30

Enhancement pattern (homogeneous/total)	12/23	4/20	.056
Presence of cystic or necrotic changes	9/23	10/20	.55
CPA : IAC	16 : 7	16 : 4	.50
Presence of adjacent parenchymal edematous change (CPA case)	5/16	8/16	.47

Values are described as median (interquartile range). CPA, cerebellopontine angle; IAC, internal auditory canal; NA, not applicable, p-value < 0.05 was considered to be statistically significant.

Table 2: Comparison of DWI and DCE-MRI quantitative parameters between CPA/IAC schwannomas and metastases

	Schwannomas (n=23)	Metastases (n=20)	p-value
nADCmean	1.69 (1.55–2.0)	1.43 (1.12–1.61)	.002
Vp	0.05 (0.03–0.09)	0.20 (0.13–0.23)	<.001
Ktrans (minute^{-1})	0.18 (0.12–0.23)	0.22 (0.15–0.41)	.51
Kep (minute^{-1})	0.41 (0.36–0.48)	0.81 (0.62–1.24)	<.001

Values are described as median (interquartile range). n, number; CPA, cerebellopontine angle; IAC, internal auditory canal; nADCmean, normalized mean apparent diffusion coefficient; Vp, blood plasma volume; Kep, flux rate constant; Vp (blood plasma volume, Ktrans, forward volume transfer constant; Kep, flux rate constant, p-value < 0.05 was considered to be statistically significant.

Table 3: Diagnostic performance of DWI and DCE-MRI quantitative parameters between CPA/IAC schwannomas and metastases

	nADCmean	Vp	Kep (minute^{-1})
Cut-off	1.68	0.12	0.53
Sensitivity	0.57 (0.35–0.77)	1.0 (0.79–1.0)	0.83 (0.61–0.95)
Specificity	0.90 (0.68–0.99)	0.75 (0.51–0.91)	0.80 (0.56–0.94)
PPV	0.87 (0.60–0.98)	0.82 (0.63–0.94)	0.83 (0.61–0.95)
NPV	0.64 (0.44–0.81)	1.0 (0.70–1.00)	0.80 (0.56–0.94)
Accuracy	0.72 (0.56–0.85)	0.88 (0.75–0.96)	0.81 (0.67–0.92)
AUC	0.77 (0.60–0.98)	0.90 (0.81–1.0)	0.83 (0.70–0.96)

nADCmean, normalized mean apparent diffusion coefficient; Vp, blood plasma volume; Kep, flux rate constant; PPV, Positive predictive value; NPV, Negative predictive value; AUC, Area under the curve; Interquartile ranges represent 95% confidence interval.

Figures

Figure 1

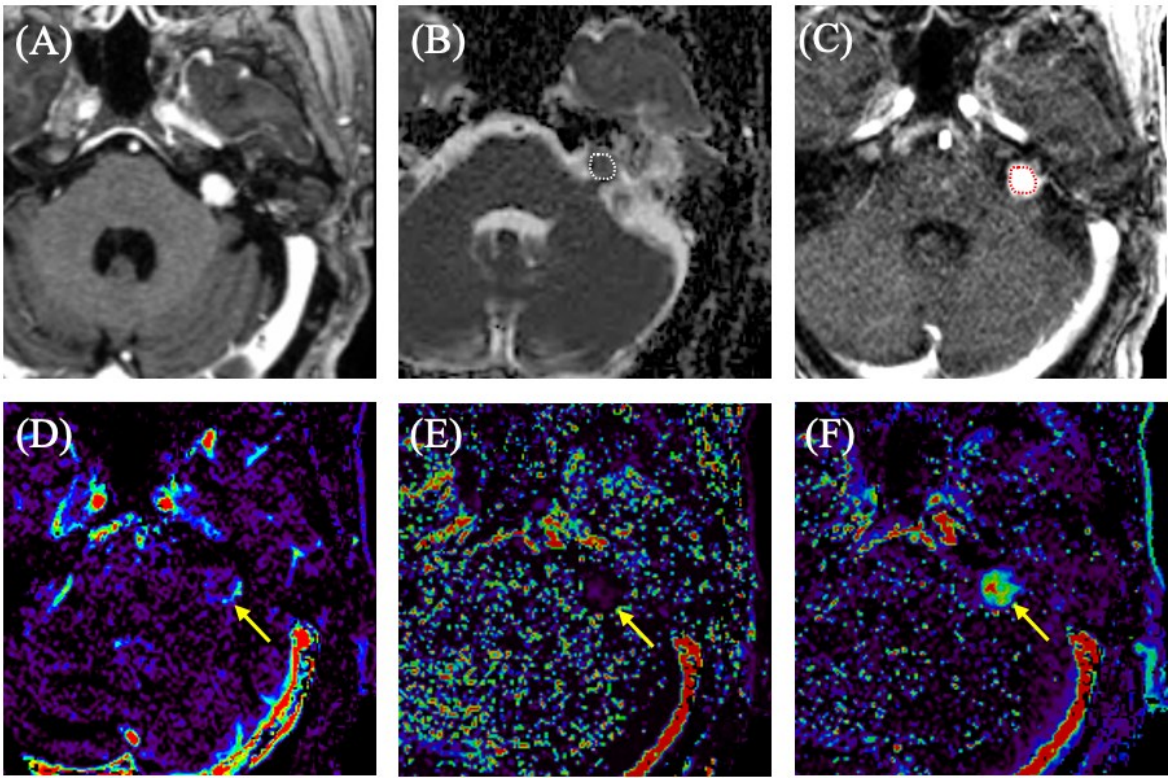

Fig. 1–A 67-year-old female with a schwannoma in the left internal auditory canal (IAC). (A) Post-contrast T1-weighted image shows a homogeneously enhancing lesion in the left IAC. (B) A region of interest (ROI) was placed on the solid component of the tumor on the apparent diffusion coefficient (ADC) map and normalized mean ADC was calculated. (c) As well, a ROI was also placed

on the permeability map, and (D) Vp (blood plasma volume), (E) Kep (flux rate constant), and (F) Ktrans (forward volume transfer constant) map were created. The corresponding values of Vp, Kep, and Ktrans (arrows) were 0.04, 0.53, and 0.5, respectively. Colors of parameters: black, low value; green, intermediate value; red, high value

Figure 2

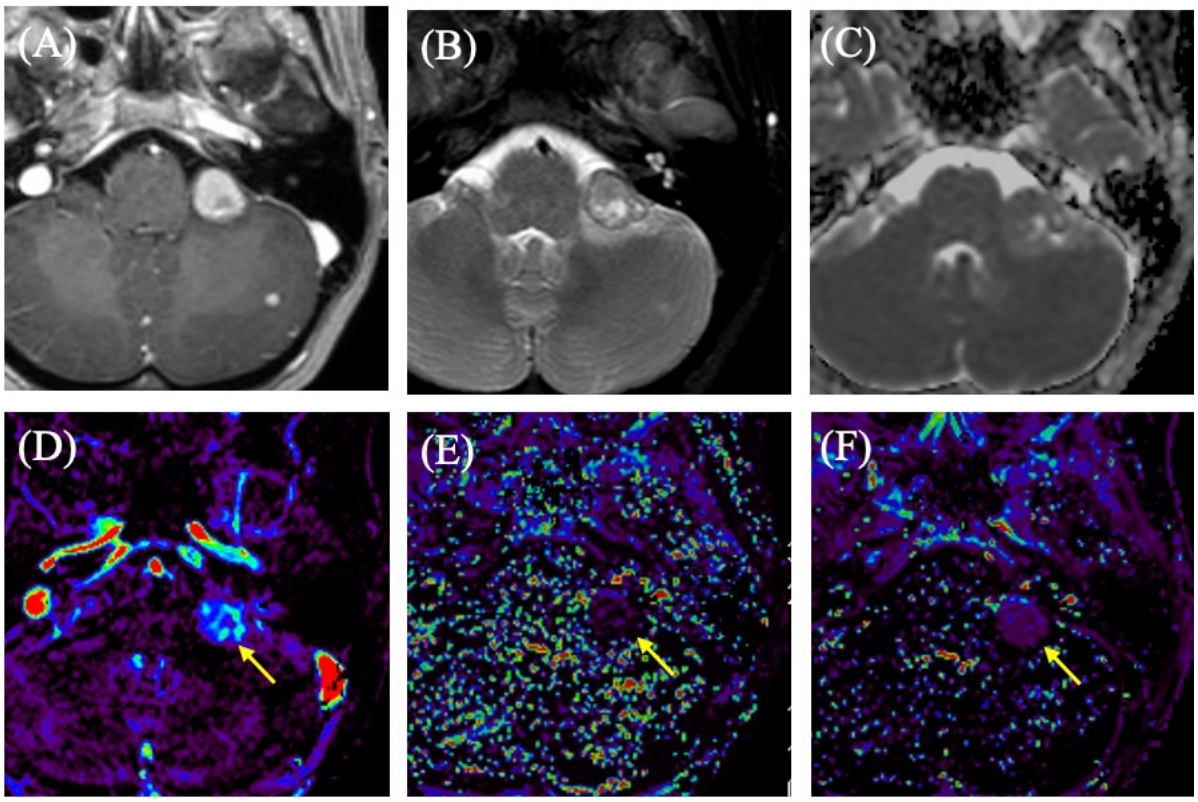

Fig. 2–A 32-year-old female with a metastatic lesion from melanoma in the left cerebellopontine angle (CPA).

(A) Post-contrast T1-weighted image shows a heterogeneously enhancing lesion in the left CPA. (B) T2-weighted image shows a cystic component within the mass and edematous changes in the

adjacent left cerebellum. (C) A region of interest (ROI) was placed on the solid component of the mass. Normalized mean apparent diffusion coefficient was 1.09. (D, E, F) A ROI was placed on the permeability map, and Vp (blood plasma volume), Kep (flux rate constant), and Ktrans (forward volume transfer constant) were calculated (arrows). Vp, Kep, and Ktrans were 0.19, 0.67, and 0.13, respectively.

Colors of parameters: black, low value; green, intermediate value; red, high value

Figure 3

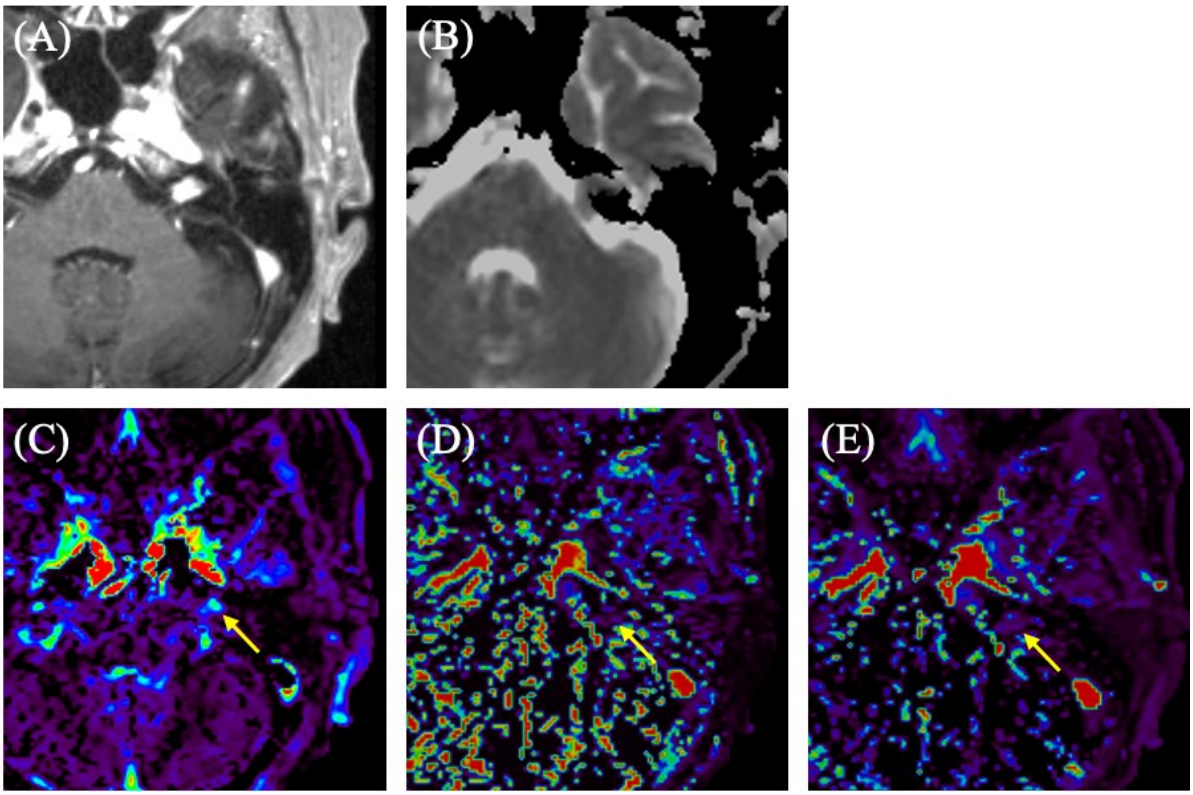

Fig. 3–A 32-year-old female with a metastatic lesion from breast cancer in the left internal auditory canal (IAC). (A) Post-contrast T1-weighted image shows a homogeneously enhancing lesion in the

left IAC. (B) On apparent diffusion coefficient (ADC) map, normalized ADC mean is 1.07. (C, D, E) A region of interest was placed on the solid component on the permeability map. Blood plasma volume, flux rate constant, and forward volume transfer constant (arrows) were 0.21, 1.08, and 0.29, respectively.

Colors of parameters: black, low value; green, intermediate value; red, high value

Figure 4

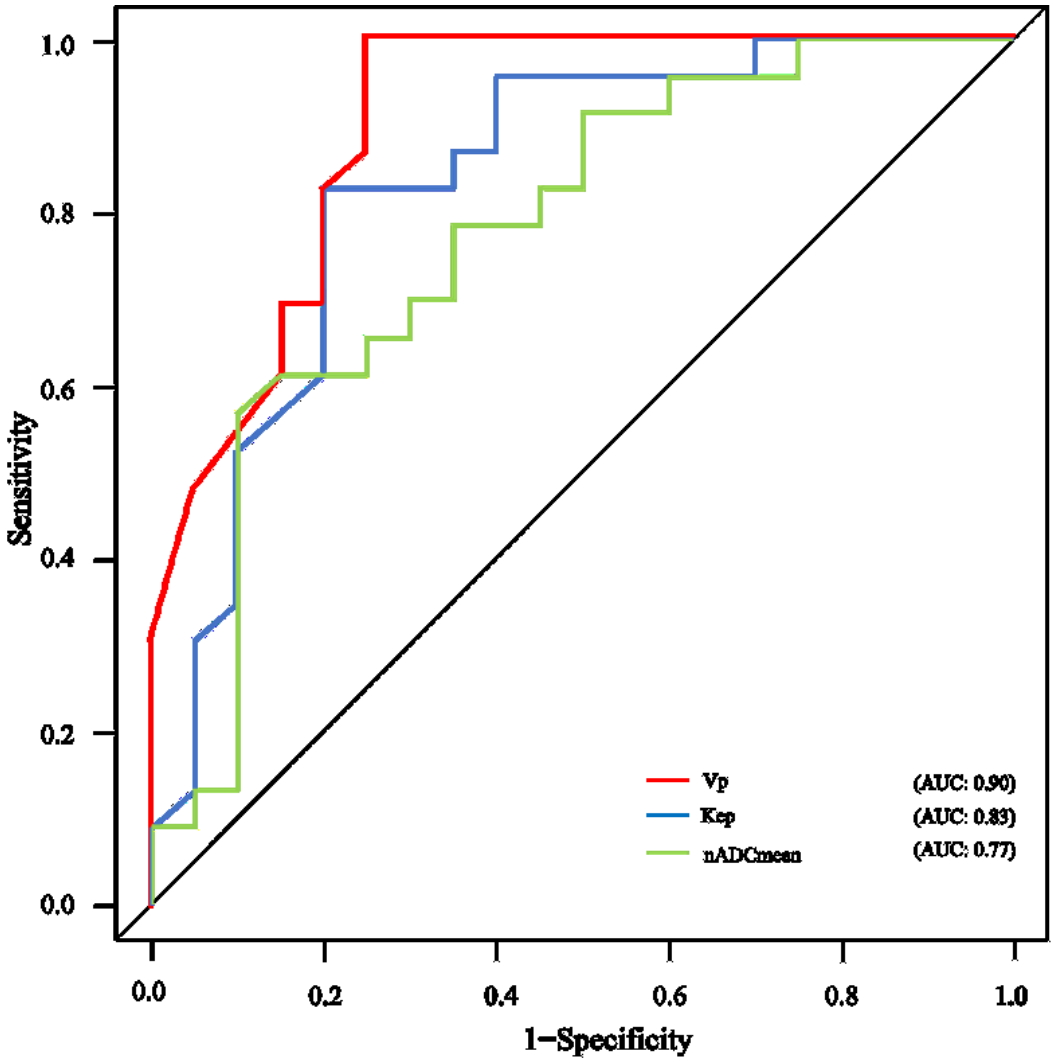

Fig. 4– Receiver operating characteristics curves of statistically significant parameters between metastases and schwannomas in diffusion-weighted imaging and dynamic contrast-enhanced MRI analyses.

Vp, blood plasma volume; Kep, flux rate constant; nADCmean, normalized mean apparent diffusion coefficient; AUC, area under the curves